Nano Energy 68 (2020) 104329

Contents lists available at ScienceDirect

Nano Energy

journal homepage: http://www.elsevier.com/locate/nanoen

Full paper

Creating visible-to-near-infrared mechanoluminescence in mixed-anion compounds $SrZn_2S_2O$ and SrZnSO

Changjian Chen [a], Yixi Zhuang [a,*], Dong Tu [b], Xiandi Wang [c], Chaofeng Pan [c], Rong-Jun Xie [a,**]

[a] College of Materials, Xiamen University, Simingnan-Road 422, Xiamen, 361005, PR China
[b] School of Physics and Technology, Wuhan University, Wuhan, 430072, PR China
[c] Beijing Institute of Nanoenergy and Nanosystems, Chinese Academy of Sciences, Beijing, 100083, China

ARTICLE INFO

Keywords:
Mechanoluminescent materials
Rare-earth-doped materials
Mixed-anion compounds
Stress sensing
Energy conversion

ABSTRACT

Mechanoluminescence (ML) materials featuring light emission in response to mechanical stimulus have shown promising applications in damage diagnosis, dynamic force detection, and information storage. However, their applications are greatly limited by a very small number of available ML materials as well as unsatisfied ML spectra. In this paper, we developed novel ML materials with intense ML and super-broad visible-to-near-infrared (470–1600 nm) spectra by incorporating lanthanide ions or transition metals into mixed-anion compounds $SrZn_2S_2O$ and SrZnSO. These mixed-anion compounds show a linear relationship between ML intensity and applied force, allowing them to be used in non-contact/multi-touch stress sensing. Moreover, the mixed-anion compounds exhibit multiband near-infrared ML enabling a significant bright-field stress sensing approach without the interference of ambient light. This work offers a unique insight for discovering new ML materials and enriching the ML spectral range, thereby promoting their potential applications in stress intelligent sensors, electronic skins, and human-machine interfaces.

1. Introduction

Mechanoluminescence (ML) materials showing light emission under mechanical stimulus have attracted striking attentions in widespread applications including E-signature systems, artificial skins, light-emitting fabric, information storage, anti-counterfeiting and optical imaging [1–6]. Since the first discovery of the ML phenomenon in 1600, a large diversity of inorganic and organic ML materials were reported, but most of those ML materials are not practically used because of their weak ML response and destructive characteristics [7–9]. Only a few discovered materials with intense and self-recoverable ML in the visible (VIS) range, *e.g.* $SrAl_2O_4:Eu^{2+}$ and $ZnS:Cu^{+}$, have finally entered into the above-mentioned application fields [5,10]. Unfortunately, these materials do not contain enough spectral components in the near-infrared (NIR, 900–1700 nm) region. The stress sensing method by using them (mainly based on the VIS ML) must eliminate the interference of ambient light. At present, the longest ML at 1390 nm was reported by Peng [11]. For the applications in biological imaging and bright-field stress sensing, high-brightness ML materials with much longer NIR emissions are highly required and need to be developed urgently.

A big challenge to discover new ML materials is the shortage of systematical research strategies. Mixed-anion compounds are a kind of solid-state materials that contain multiple anionic species in a single phase, such as oxynitrides and oxychalcogenides [12]. They have drawn great interests of chemists, physicists, and material scientists because they are widely applied in catalysis, energy conversion, and electronic devices [13–15]. These mixed-anion compounds are regarded as interesting and promising materials because they may support novel chemical and physical phenomena inaccessible to single-anion materials, such as crystal field splitting, binding energy differentiating and local symmetry breaking, due to difference in ionic radius, charge, electronegativity and polarizability of each anion [16–18]. Notably, the reduction of local symmetry may induce the formation of noncentrosymmetry (polarization) and piezoelectricity of crystalline materials [19], which have been confirmed in the compounds containing $MQ_{4-x}O_x$ (M = Zn, V, Fe, Co, and Ga; Q = Se, Te, and S) tetrahedral building blocks [12,20,21]. Since the recoverable ML is dominantly contributed to a coupling effect of piezoelectricity and photoexcitation (*i.e.* piezophotonic effect) [22–25], the mixed-anion compounds may become a significant and abundant family of ML materials. However, investigations on

* Corresponding author.
** Corresponding author.
E-mail address: zhuangyixi@xmu.edu.cn (Y. Zhuang).

https://doi.org/10.1016/j.nanoen.2019.104329
Received 27 October 2019; Received in revised form 20 November 2019; Accepted 25 November 2019
Available online 29 November 2019

mixed-anion compounds as ML materials are extremely limited. Especially, the relationship between the mixed-anion building blocks and the ML properties is still unclear.

Here we propose an approach to explore novel ML materials and to achieve tunable ML spectra in an ultra-wide spectral range (Fig. 1). A local asymmetry is generated by replacing single-anion ligands with multiple-anion species in coordinating tetrahedra or octahedra (Fig. 1a–i). The local asymmetry is evolved to an overall non-centrosymmetry (piezoelectricity) in a crystalline compound with periodically aligned mixed-anion building blocks when the net polarization is retained in a primary unit (Fig. 1a–ii). Furthermore, multi-color ML can be created by incorporating various luminescent ions such as lanthanide ions (Ln) or transition metals (TM) into these mixed-anion compounds, which couples the piezoelectricity with photoexcitation and produces an effective stress-to-photon conversion process (Fig. 1a–iii).

In this paper, we successfully developed high-performance ML materials in several mixed-anion compounds like $SrZn_2S_2O$, SrZnSO, β-SiAlON and $SrSi_2O_2N_2$ that all contain tetrahedral mixed-anion building units. Tunable spectra in an ultra-wide spectral range from 470 to 1600 nm in these ML materials were realized (Fig. 1b). We demonstrated multi-color and multi-touch dynamic force detection benefited from the tunability of ML spectra, and then established a bright-field stress sensing approach without the interference of ambient light by using NIR ML films and NIR detectors (Fig. 1c). The concept to discover novel ML materials in mixed-anion compounds can be extended to other materials in the abundant mixed-anion families. Therefore, this work provides a feasible solution to the limited number and unsatisfied spectral range of ML materials in the applications of stress intelligent sensors, electronic skins, and human-machine interfaces.

2. Results and discussion

2.1. Crystal structure and local coordination structure

XRD patterns of the as-synthesized phosphors $SrZn_2S_2O:Mn^{2+}$ and $SrZnSO:Pr^{3+}$ match well with the standard cards (Fig. 2a and Fig. S2a), which indicates that a low concentration of dopants (~1%) does not obviously change the crystal structure. The SEM images show the particle size of $SrZn_2S_2O:Mn^{2+}$ and $SrZnSO:Pr^{3+}$ is about 5 and 20 μm, respectively (Fig. 2b and Fig. S2b). The EDX spectroscopic mapping on a randomly selected particle of $SrZn_2S_2O:Mn^{2+}$ (Fig. 2c) and SrZnSO: Pr^{3+} (Fig. S2c) confirm a highly homogeneous distribution of the Mn^{2+} and Pr^{3+} in both hosts. According to the XRD characterization, the $SrZn_2S_2O$ crystallizes in an orthorhombic space group of $Pmn2_1$ (No. 31). The two-dimensional structure of $SrZn_2S_2O$ is composed of closed-packed corrugated double layers of tetrahedral ZnS_3O vertically separated by Sr^{2+} ions (Fig. 2d). In addition, the tetrahedral ZnS_3O connected by a common shared sulfur apex has two distinct orientations, contributing to noncentrosymmetric polar behavior. The $SrZn_2S_2O$ host provides Sr^{2+} sites (1.18 Å, coordination number (CN) = 6) and Zn^{2+} sites (0.60 Å, CN = 6) for the accommodation of lanthanide ions and transition metals, respectively. The hexagonal SrZnSO exhibits a layered structure and crystallizes in a space group of $P6_3mc$ (No. 186). The parallel-arranged tetrahedral ZnS_3O units are separated by Sr^{2+} ions, resulting in a polar z-direction and piezoelectric effect (Fig. 2e) [26].

2.2. Photoluminescence properties

The non-doped $SrZn_2S_2O$ samples shows an obvious drop of reflectance in 250–400 nm, corresponding to the band-to-band transition of the host (Fig. 3a). The optical band gap of the $SrZn_2S_2O$ host is evaluated

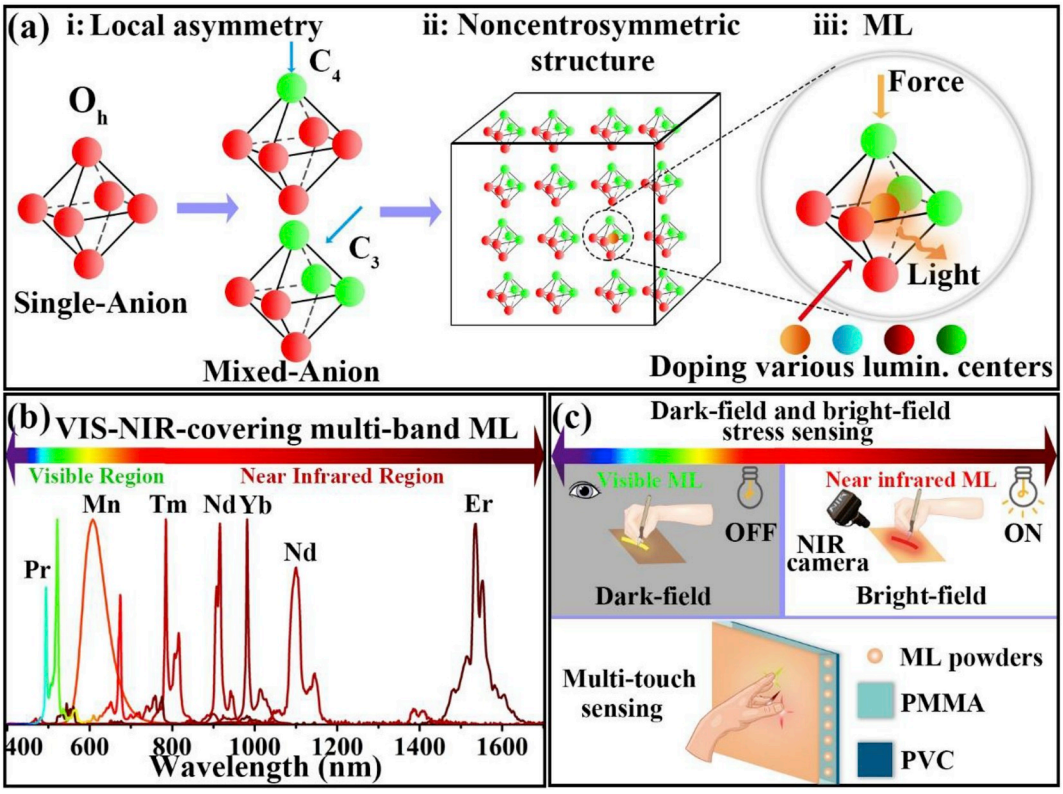

Fig. 1. Design route and applications of ML materials in mixed-anion compounds. (a–i) Formation of local asymmetry, *e.g.* C_4 or C_3 through replacing one and three ligands by other anion species. (a-ii) An overall noncentrosymmetric structure constructed by periodically aligned mixed-anion polyhedrons. (a-iii) Creation of multi-color ML by doping various luminescent centers in mixed-anion compounds. (b) Multiband ML spectra covering the whole VIS-NIR region in Ln^{3+}- or Mn^{2+}-doped SrZnSO. (c) Various applications of multi-color ML materials. The VIS ML materials can be applied to a conventional dark-field stress sensing. The NIR ML materials offers an advanced stress sensing approach operable under the natural light (bright-field sensing).

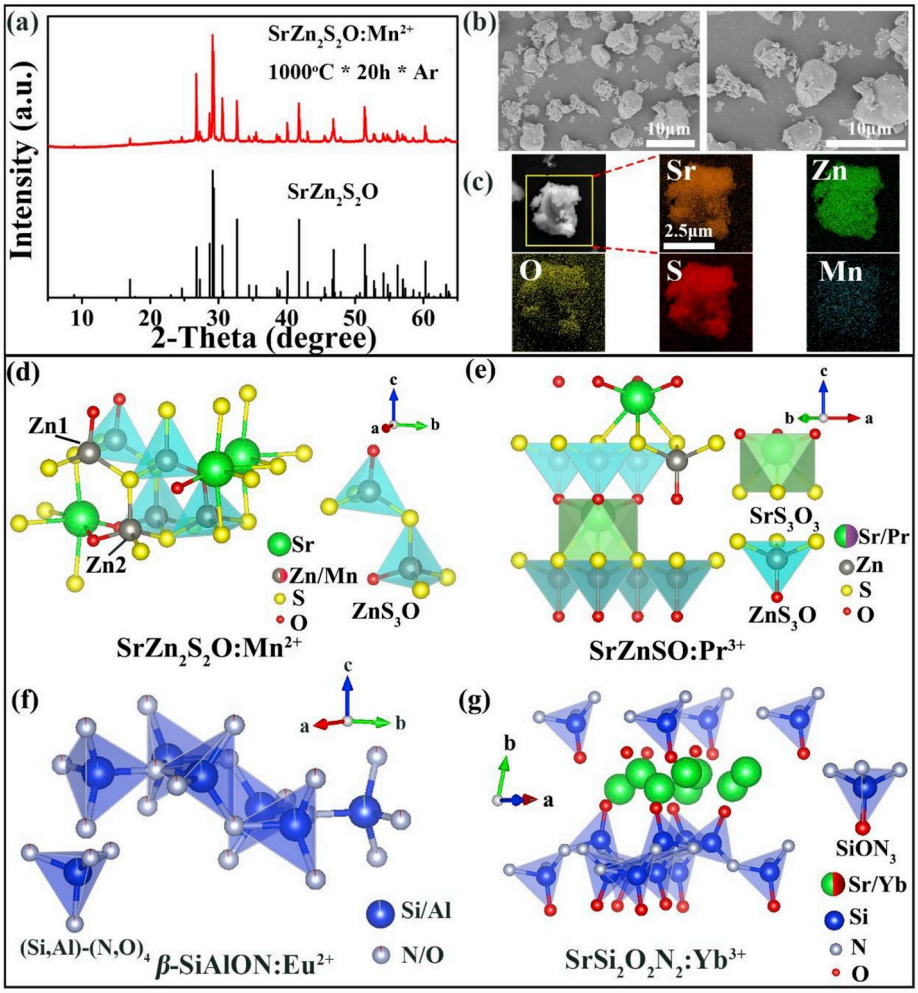

Fig. 2. Structural and morphological characterizations. (a) XRD patterns, (b) SEM images and (c) EDX elemental distribution mapping of the $SrZn_2S_2O:Mn^{2+}$ sample. (d–g) Crystal structures of $SrZn_2S_2O$ (d), SrZnSO (e), β-SiAlON (f), and $SrSi_2O_2N_2$ (g). The crystals are constructed by mixed-anion tetrahedral building units of ZnS_3O, $(Si,Al)\text{-}(O,N)_4$, or $SiON_3$.

to be 3.82 eV according to the Kubelka–Munk method and Tauc plot (inset of Fig. 3a), which is in a good agreement with the value reported by Tsujimoto et al. (3.86 eV) [21]. The Mn^{2+}-doped $SrZn_2S_2O$ sample shows several excitation bands in 400–600 nm due to d-d transitions of Mn^{2+} and broad bands in 250–350 nm (Fig. 3b). The broad excitation bands are composed of a charge transfer state (CTS) of Mn^{2+} and the band-to-band transition of the host, indicating a possible energy transfer route from the host to Mn^{2+}. $SrZn_2S_2O:Mn^{2+}$ exhibits a yellow emission peaked at 584 nm due to the Mn^{2+}: $^4T_1(^4G) \rightarrow {}^6A_1(^6S)$ transition. The lifetime of the yellow emission at RT is about 1.5 ms (Fig. 3c). The thermal quenching temperature (T50%, the temperature where the intensity is quenched to 50% of the initial intensity) is 360 K for $SrZn_2S_2O:Mn^{2+}$ (Fig. 3d). Besides the transition metals, we also successfully incorporated trivalent lanthanide ions into the $SrZn_2S_2O$ host, and created various PL according on the f-f transitions of lanthanide ions (Fig. S3).

Similarly, the optical band gap of SrZnSO is estimated to be 3.96 eV (Fig. 3e). As an example, the $SrZnSO:Pr^{3+}$ sample shows typical PL peaks at 494, 522, 674, 759 and 775 nm due to the f-f transitions (Fig. 3f). The PLE spectrum of $SrZnSO:Pr^{3+}$ shows intense absorptions in 250–320 nm, which could be majorly originated from the band-to-band transition. The photoluminescence properties indicate that the $SrZn_2S_2O$ and SrZnSO are excellent hosts for accommodating both lanthanide ions and transition metals, which are indispensable to achieve multi-color PL and ML as will be discussed blow.

2.3. Mechanoluminescence properties

Interestingly, the mixed-anion compounds of the Ln^{3+}-doped or TM^{2+}-doped $SrZn_2S_2O$ and SrZnSO show bright emissions upon mechanical stimulus. $SrZn_2S_2O:Mn^{2+}$ exhibits an orange-red ML peaked at 597 nm (Fig. 4a, top), similar to its PL but with a red shift of 13 nm (Fig. 4a, bottom). The red shift of ML emission could be attributed to two different Zn^{2+} sites for Mn^{2+} substitution in $SrZn_2S_2O$ (Fig. 2d). SrZnSO:Pr^{3+} shows a green ML emission with several sharp peaks at 494, 522, 674, 759, and 775 nm (Fig. 4b, top), matching well with the PL spectrum (Fig. 4b, bottom). The photographic images of the $SrZn_2S_2O:Mn^{2+}$ and $SrZnSO:Pr^{3+}$ phosphors under natural light (NL), under 254 nm excitation, and upon rubbing in the dark are given in the insets of Fig. 4a and b. The bright ML emission is clearly observed by naked eyes when the phosphors are gently rubbed by using a glass rod. The relationship between the ML intensity and the loaded pressure was studied by applying different forces onto the composite cylinders. Both of $SrZn_2S_2O:Mn^{2+}$ and $SrZnSO:Pr^{3+}$ show a linear increase of ML intensity on the compressive force in a wide range (Fig. S4), allowing them to be applied for stress sensing.

We also prepared mixed-anion compounds in oxynitride families and found new ML materials of β-$SiAlON:Eu^{2+}$ and $SrSi_2O_2N_2:Ln^{3+}$ (Fig. S5). The XRD characterization indicates that β-SiAlON is derived from β-Si_3N_4 by the partial substitution of Si by Al and N by O. Local asymmetry could be generated from the $(Si,Al)\text{-}(N,O)_4$ mixed-ion tetrahedral

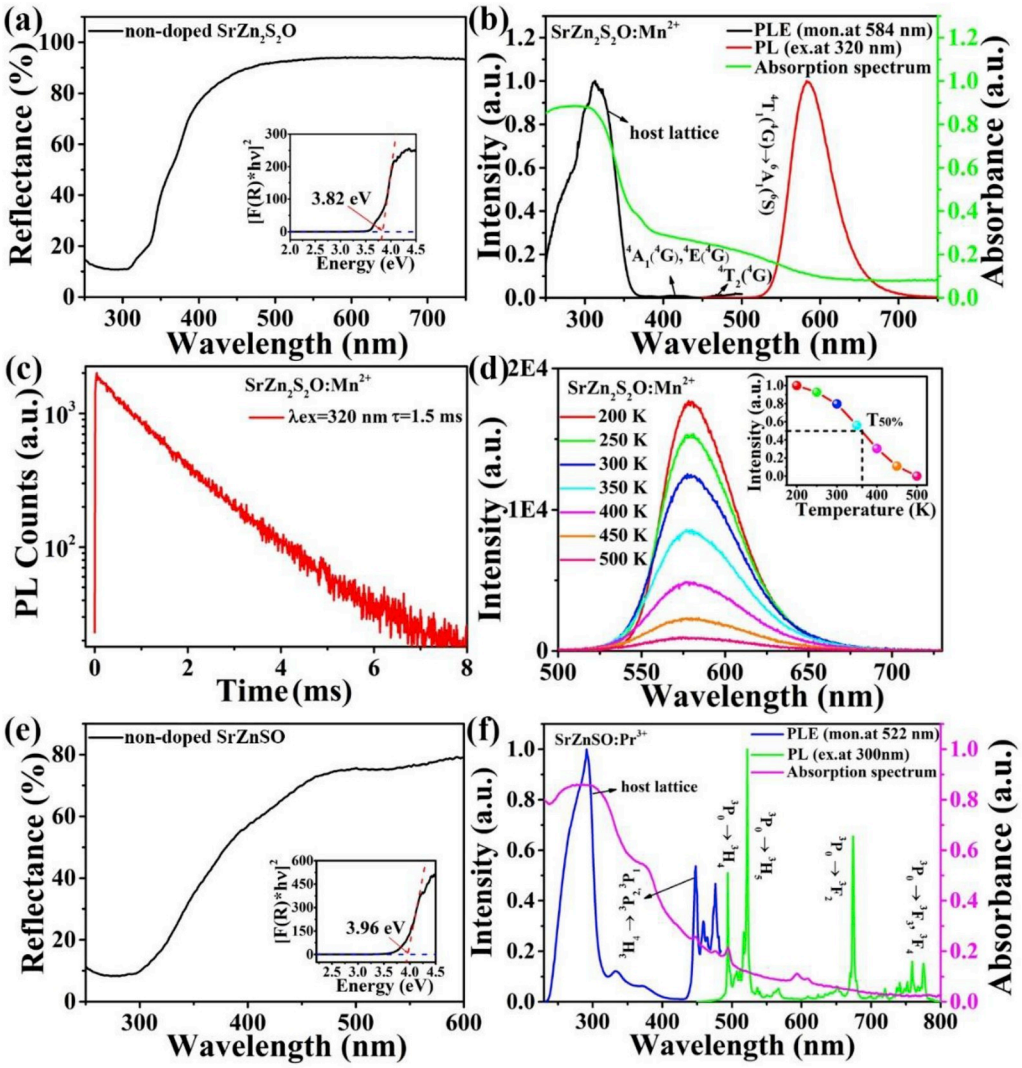

Fig. 3. Photoluminescence properties. (a) Diffuse reflectance spectra of the non-doped $SrZn_2S_2O$. The inset shows the Tauc plot and the estimated optical band gap for $SrZn_2S_2O$. (b) Absorption, PLE (monitoring at 584 nm), and PL (excited at 320 nm) spectra of $SrZn_2S_2O$:Mn^{2+}. (c) PL decay curves of $SrZn_2S_2O$:Mn^{2+} monitored at 583 nm upon excitation at 320 nm. (d) Temperature-dependent PL spectra of $SrZn_2S_2O$:Mn^{2+} under 310 nm excitation. The inset shows the integrating PL intensity as a function of temperature. T50% is defined as the temperature where the intensity is quenched to 50% of the initial intensity. (e) Diffuse reflectance spectra of the non-doped SrZnSO. The inset shows the Tauc plot and the estimated optical band gap for SrZnSO. (f) Absorption, PLE (monitoring at 522 nm), and PL spectra (excited at 300 nm) of SrZnSO:Pr^{3+}.

(Fig. 2f) [15]. $SrSi_2O_2N_2$ consists of layered $SiON_3$ tetrahedrons and Sr^{2+} atoms, belonging to a space group of P1 (No. 1). The polarization of $SiON_3$ tetrahedrons is not totally cancelled out, therefore keeps non-centrosymmetry and piezoelectricity in $SrSi_2O_2N_2$ (Fig. 2g) [27]. For the first time, green and NIR ML are discovered in mixed-anion compounds like β-SiAlON:Eu^{2+} and $SrSi_2O_2N_2$:Yb^{3+}, respectively (Fig. 4c and d). The ML spectra are consistent with their PL spectra.

Exactly, besides $SrZn_2S_2O$:Mn^{2+}, SrZnSO:Pr^{3+}, β-SiAlON:Eu^{2+} and $SrSi_2O_2N_2$:Yb^{3+}, several reported ML materials also show mixed-anion components (see Table 1), although the concept of mixed anions was not clearly proposed in previous reports. For example, a red ML has been reported in CaZnOS:Mn^{2+} (Fig. S6) [28,29]. CaZnOS is composed of layered mixed-anion polyhedral of ZnS_3O and crystallized in a piezoelectric structure (space group $P6_3mc$ (No.186)). Also, a green ML has been discovered in Eu^{2+}-doped $BaSi_2O_2N_2$ and $SrSi_2O_2N_2$ (Fig. S6) by Smet et al. [30]. Therefore, to construct local asymmetry from polarized mixed-anion units could be a feasible way to rapidly explore novel ML materials. It is worth noting that not all mixed-anion compounds guarantee intense ML. There are some requirements for realizing intense ML in a material, such as net polarization in a primary unit, suitable traps as energy relay centers, luminescent centers with high quantum efficiency, and possibly an energy transfer path from host to luminescent centers.

Possible energy conversion/transfer processes in mixed-anion ML materials are schematically illustrated by taking $SrZn_2S_2O$:Mn^{2+} as an example (Fig. 4e). $SrZn_2S_2O$ is a wide band-gap semiconductor, which is composed of tetrahedral ZnS_3O units (Fig. 1d). Under a force, the centers of anions and cations in the tetrahedral ZnS_3O are slightly separated along a certain direction, leading to a dipole moment. A macro piezoelectric potential (P) is generated in the crystal when all the tetrahedral ZnS_3O units retain a net polarization orientation. This inner piezopotential may cause the separation of charge carriers (process ① in Fig. 4e). The separated electrons and holes are captured by traps below the conduction band (CB) and those above the valence band (VB), respectively (②,③). Simultaneously, the electrons and holes are released from the traps due to tilting of energy bands under the inner piezo-potential (④). The recombination emission between the electrons and holes is resonantly transferred to Mn^{2+} ions (⑤), which pumps their electrons from the ground state to higher energy levels (⑥). Finally, after a non-radiative relaxation process (⑦), a red ML is then observed due to the $^4T_1(^4G)$ to $^6A_1(^6S)$ transition of Mn^{2+} (⑧) [22,31–33]. Nevertheless, we believe that the study on the mechanism of ML is still in its infancy. More in-depth investigations, especially on the structure-property relationships, are highly needed for the understanding of the nature of ML.

2.4. Multiband tunable ML in the whole VIS-NIR region

The wavelength coverage of ML is greatly expanded by incorporating various luminescent centers into the mixed-anion compounds (the XRD patterns are given in Fig. S7). Owning to the abundant energy levels, the

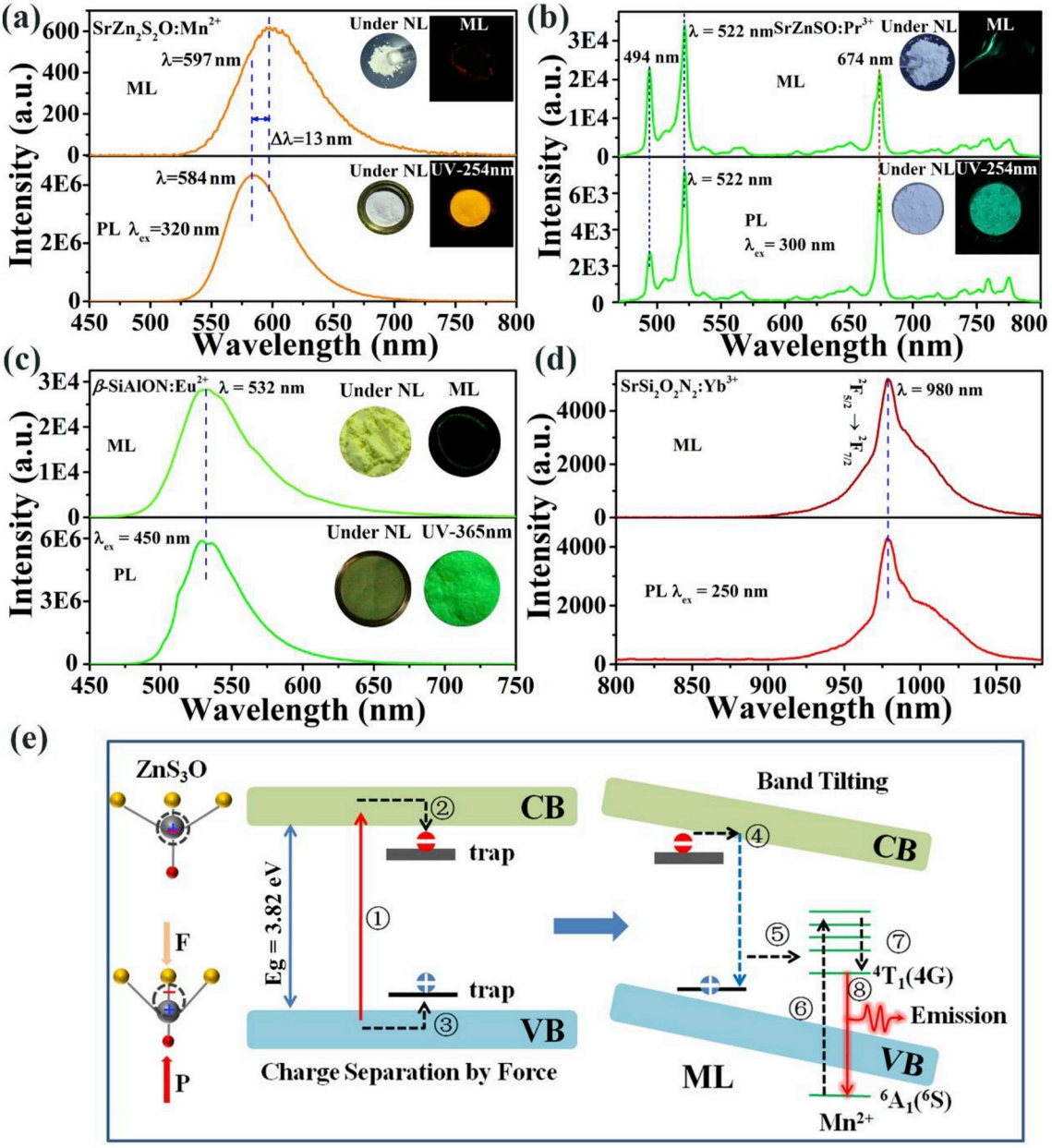

Fig. 4. ML spectra and the proposed ML mechanism. (a–d) ML (top) and PL spectra (bottom) of $SrZn_2S_2O:Mn^{2+}$ (a), $SrZnSO:Pr^{3+}$ (b), β-$SiAlON:Eu^{2+}$ (c), and $SrSi_2O_2N_2:Yb^{3+}$ (d). The insets show photographic images of the phosphors under natural light (NL), under UV excitation, and upon rubbing by using a glass rod. (e) A proposed ML mechanism of $SrZn_2S_2O:Mn^{2+}$.

Table 1
Mechanoluminescent compounds and their properties.

Composition	Crystal system	Space Group	Mixed-anion polyhedrons	References
$SrZnSO:Pr^{3+}$	Hexagonal	P 6_3mc	ZnS_3O	This work
$SrZn_2S_2O:Mn^{2+}$	Orthorhombic	P $mn2_1$	ZnS_3O	This work
β-$SiAlON:Eu^{2+}$	Hexagonal	P6_3	$(Si,Al)-(N,O)_4$	This work
$SrSi_2O_2N_2:Yb^{3+}$	Triclinic	P1	$SiON_3$	This work
$CaZnOS:Mn^{2+}$/ Ln^{3+}	Hexagonal	P 6_3mc	ZnS_3O	[6,18]
$BaSi_2O_2N_2$: Eu^{2+}	Orthorhombic	$Cmc2_1$	$SiON_3$	[19]
$SrSi_2O_2N_2:Eu^{2+}$	Triclinic	P1	$SiON_3$	[19]

Ln^{3+}- or Mn^{2+}-doped SrZnSO exhibits tunable multi-band ML spanning from green ($SrZnSO:Er^{3+}$, $SrZnSO:Ho^{3+}$, and $SrZnSO:Pr^{3+}$), yellow ($SrZnSO:Dy^{3+}$), red ($SrZnSO:Mn^{2+}$ and $SrZnSO:Sm^{3+}$), to NIR region ($SrZnSO:Tm^{3+}$, $SrZnSO:Nd^{3+}$, $SrZnSO:Yb^{3+}$, and $SrZnSO:Er^{3+}$) (Fig. 5a and b, and Table S1). The Commission International del'Eclairage (CIE) coordinates for ML in the visible region are displayed in Fig. 5c and Table S2. More importantly, we achieve the longest NIR ML at 1550 nm due to the $^4I_{13/2} \rightarrow {}^4I_{15/2}$ transition of Er^{3+}. The ML intensity of Ln^{3+}-(Ln^{3+} = Sm^{3+}, Tb^{3+}, Dy^{3+}, Ho^{3+}, Er^{3+}) and Mn^{2+}-doped samples is linearly related to the applied force (Fig. S8). The ML intensity of various doped samples under the same load at 1800 N is compared. The SrZnSO:Pr^{3+} sample shows the most intense ML in the SrZnSO series (Fig. S9). The colorful ML encourages us to apply the ML materials in advanced E-signature sensing. We used a ballpoint pen to write some Chinese characters on the surface of the ML cylinders. The motion trails of the ballpoint touching the ML cylinders were recorded by a VIS or NIR

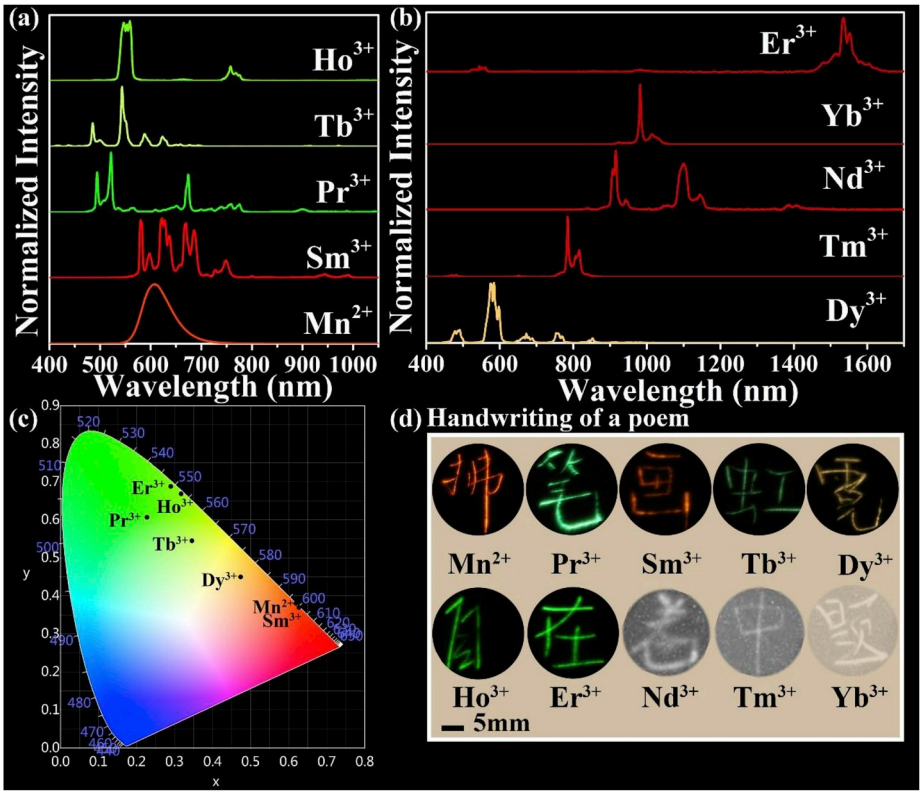

Fig. 5. Tunable multi-band ML in the VIS-NIR region. (a, b) ML spectra of SrZnSO doped with different lanthanide ions and transition metals. (c) The CIE coordinates of the multicolor ML. (d) Photographic images recording the motion trails of a ballpoint pen on the surface of the ML cylinders. The ML images exhibit various handwritten Chinese characters and different ML colors. The ten Chinese characters compose a poem (meaning: the answer of how to draw a rainbow can be found in this paper). The exposure time for each photo was 2 s.

camera in the dark (Fig. 5d). Also, the $SrZn_2S_2O$ host is available to realize tunable ML in a broader spectral region. The green ML in Pr^{3+}-doped and NIR ML in Yb^{3+}-doped $SrZn_2S_2O$ are demonstrated in Fig. S10.

2.5. Applications to multi-touch pressure sensing and bright-field stress visualization

Traditional pressure sensors based on the piezoelectric effect, resistance, or capacitance require complicated pressure sensor arrays for multi-point pressure sensing [34–36]. ML materials show great advantages on multi-touch sensing and stress visualization when coupled with commerciallized multi-channel optoelectronic devices such as charge-couple devices (CCD) or complementary metal oxide semiconductor (CMOS) sensors. We prepared a ML film by mixing the ML phosphor with PMMA and coated the film on a PVC substrate (Fig. 6a). A smooth surface of the film and excellent adhesion to the PVC substrate (Fig. S11) are confirmed in SEM images. The film shows excellent flexibility and water-resistance (Fig. 6a). Compared with a 65% drop of luminecent intensity in the $SrZnSO:Mn^{2+}$ phosphor after water sonication for 30 min, the luminescent intensity of the film remains more than 90% after sonication for 60 min (Fig. S12). The multi-touch pressure sensing is demonstrated by pressing the ML film on a 4 × 4 array of nails (Fig. 6b). The spatial distribution of the applied pressure on the ML film is visualized in Fig. 6c. The applied pressure could be derived from the ML intensity for each point in the pseudo-color image because of the linear relationship between the force and ML intensity (Fig. 6d and e). Moreover, the multi-touch pressure sensing in a dynamic mode is demonstrated by drawing two trajectories on the ML film. The dynamic ML images are recorded in Video S1, and several frames are extracted from the video with an interval of 0.2 s in Fig. S13. The pressure and speed of two trajectories are clearly revealed by the dynamic ML.

Supplementary video related to this article can be found at https://doi.org/10.1016/j.nanoen.2019.104329

At present, the stress visualization is mainly based on visible ML materials such as $ZnS:Mn^{2+}$ [1] or $SrAl_2O_4:Eu^{2+}$ The visible ML should be detected in a dark field in order to cut off the signal interference from the ambient visible light. In this paper, we proposed a bright-field stress sensing approach by using NIR ML materials ($SrZnSO:Er^{3+}$, $\lambda = 1534$ nm) and a NIR detector without the need to shield the visible light. Fig. 6f shows a VIS camera (left) and a NIR camera (right) simultaneously recording a $SrZnSO:Er^{3+}$ ML film in a bright field. When rubbing on the film, the VIS ML signals are totally submerged in the ambient light (Fig. 6g); on the other hand, intense NIR ML signals are clearly recorded in the NIR camera (Fig. 6h and Video S2). The bright-field stress sensing by using NIR ML materials and NIR detectors offer a new stress sensing approach without the interference of ambient light. The NIR-ML-based bright-field stress sensing greatly improve the sensitivity of detection and simplify the requirement of measurement, therefore showing great promises in the applications of structure damage diagnosis, electronic skin, and human-machine interface.

Supplementary video related to this article can be found at https://doi.org/10.1016/j.nanoen.2019.104329

3. Conclusions

In summary, this work provided a new concept and solution to explore ML materials and to expand the ML spectral range. By incorporating lanthanide ions or transition metals into mixed-anion compounds ($SrZn_2S_2O$, SrZnSO, β-SiAlON, and $SrSi_2O_2N_2$ as discussed in this work), novel ML materials showing tunable ML in a super-wide wavelength range (470–1600 nm) were successfully synthesized. The local asymmetry from the mixed-anion polyhedra, suitable traps, luminescent centers, and possibly an efficient energy transfer path from host to luminescent centers were considered to be key components for achieving intense ML. We fabricated a ML film showing excellent ML property, flexibility and water-resistance by scraping the developed ML phosphor with PMMA on the PVC substrate. We demonstrated the applications of the wavelength-tunable ML film in both static and dynamic multi-touch stress sensing. Furthermore, we proposed a new bright-field

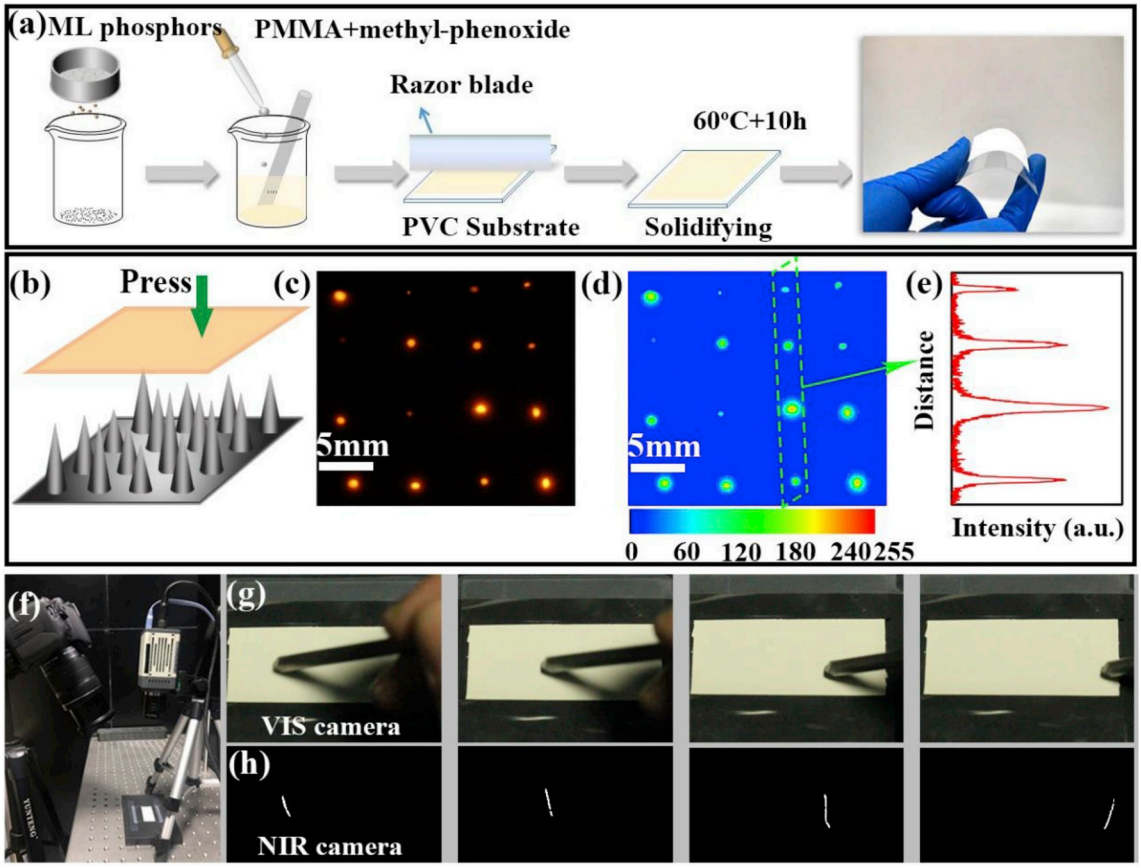

Fig. 6. Applications to the multi-touch pressure sensing and bright-field stress visualization. (a) Schematic diagram for the preparation of ML film. The film shows excellent flexibility and water-resistance. (b) Schematic illustration for the application of the multi-touch pressure sensing by pressing a ML film on a 4 × 4 array of nails. (c) A ML image acquired under pressing. The ML image visualizes the pressure distribution on the film. The different ML intensity is originated from different length (stress) of the nails. (d) A pseudo-color image showing the spatial distribution of pressure. (e) Relative ML intensity along a straight line as marked in (d). (f) Bright-field stress sensing by using a NIR camera (right) to monitor optical signals from a NIR ML film (bottom). Another VIS camera (left) is set up to record optical signals for comparison. (g,h) Photographic images taken from the VIS (g) and NIR camera (h), respectively. When rubbing on the film, the VIS ML signals are totally submerged in the ambient light. On the other hand, intense NIR ML signals are clearly recorded by the NIR camera.

stress sensing approach by using NIR ML materials and a NIR detector. This approach eliminated the interference of the ambient light, which is a big problem for the normal VIS-ML-based stress sensing. Considering the variety of mixed-anion material families, we expect that this work may provide a guidance for creating more ML materials and devices, thereby greatly promote the applications of ML materials in pressure sensing, human-machine interfaces, anti-counterfeiting, and damage diagnosis.

4. Experimental section

4.1. Chemicals and materials

Chemical reagents $SrCO_3$ (3.5 N) and SiO_2 were purchased from Sinopharm Corporation; Si_3N_4 (>95%) was received from UBE Corporation; ZnS (4 N), Li_2CO_3 (4 N), ZnO (4 N), anisole solution (AR) were purchased from Aladdin Corporation; rare-earth oxides Pr_2O_3 (4 N), Nd_2O_3 (4 N), Sm_2O_3 (4 N), $Tb_2(CO_3)_3$ (4 N), Dy_2O_3 (4 N), Ho_2O_3 (4 N), Er_2O_3 (4 N), Tm_2O_3 (4 N), Yb_2O_3 (4 N) were supplied by Zhongnuoxincai (Beijing) Corporation. A commercial phosphor β-SiAlON:Eu^{2+} was provided by Beijing Yuji Science & Technology Corporation. PMMA (poly (methyl methacrylate)) microspheres and PVC (Polyvinyl chloride) was purchased from Mitsubishi Rayon Polymer Corporation and Cloud Zhuo Crafts Corporation, respectively. Al_2O_3 crucibles (>99%, Φ28 mm × 17 mm) were used as sample holders in the sintering process.

4.2. Synthesis of mechanoluminescence materials

All the samples were prepared by the high-temperature solid-state reaction method. In the synthesis of Mn^{2+}/Ln^{3+}-doped SrZnSO, stoichiometric $SrCO_3$, ZnS, and $MnCO_3$ or Ln_2O_3 (Ln = Pr, Nd, Sm, Tb, Dy, Ho, Er, Tm, or Yb) according to the compositions of $Sr_{0.99}Ln_{0.01}ZnSO$ or $SrZn_{0.99}Mn_{0.01}SO$ with additional 1 wt % Li_2CO_3 as sintering flux were homogeneously mixed and ground in an agate mortar (unless otherwise stated, the activator concentration is 1 mol% of ZnS or $SrCO_3$). The mixtures were transferred into Al_2O_3 crucibles and sintered at 1050 °C for 8 h in a horizontal tube furnace under argon atmosphere. For the synthesis of Mn^{2+}/Yb^{3+}/Pr^{3+}-doped $SrZn_2S_2O$, stoichiometric $SrCO_3$, ZnS, and $MnCO_3$ or Ln_2O_3 (Ln = Pr or Yb) were homogeneously mixed, ground, and subsequently sintered in an alumina crucible at 1000 °C for 24 h in a horizontal tube furnace under argon atmosphere to obtain $SrZn_{1.99}Mn_{0.01}S_2O$ or $Sr_{0.99}Ln_{0.01}Zn_2S_2O$. For the synthesis of $SrSi_2O_2N_2$:0.01 Yb^{3+}, $SrCO_3$, SiO_2, and Yb_2O_3 were homogeneously mixed and sintered at 1300 °C for 3 h in a horizontal tube furnace under a reducing atmosphere (H_2/N_2:5%/95%) to obtain Sr_2SiO_4:Yb precursors. After cooling down to room temperature, the obtained powders were further mixed and ground with appropriate amounts of Si_3N_4 and then calcined at 1550 °C for 6 h in a horizontal tube furnace under the same reducing atmosphere.

4.3. Preparation of ML cylinders and ML films

In order to evaluate the ML performance, composite ML cylinders (25 mm in diameter and 10 mm in thickness) were prepare by mixing screened phosphors (through 300 meshes) with transparent epoxy resin (SpeciFix, Struers GmbH) under a mass ratio of 1:9. Composite ML films were prepared by using a blade-coating method. Screened particles of SrZnSO:Mn or SrZnSO:Er phosphors were mixed with PMMA in anisole solution to form a homogeneous paste. A layer of transparent PVC film with 2 mm thickness was cut into 5 × 5 cm pieces as a flexible substrate. Four stacks of Scotch tape (45 μm in thickness) was adhered along the two opposite edges of the substrate. Then the paste was dispensed onto the substrate and scraped along the Scotch tape using a razor blade. Finally, the paste films were solidified at 60 °C for 10 h in air.

4.4. Structural and optical characterizations

X-ray powder diffraction (XRD) patterns were acquired by an X-ray diffractometer (D8 ADVANCE, Bruker) with Cu Kα radiation (λ = 0.15406 nm) at 40 kV and 40 mA. The surface morphology and elemental mapping were characterized by a field-emission scanning microscope (SU70, Hitachi) equipped with an energy-dispersive X-ray (EDX) spectroscope system. Photoluminescence emission (PL), photoluminescence excitation (PLE) and PL decay curves were measured in a fluorescence spectrophotometer (FLS980, Edinburgh Instruments). Diffuse reflectance spectra were measured with a UV–Vis spectrophotometer (UV-3600 Plus, Shimadzu). The temperature-dependent luminescence spectra were performed by combining a cooling/heating stage, (THMS600E, Linkam Scientific Instruments) and a charge-coupled device (CCD) spectrometer (USB2000+, Ocean Optics). The ML spectra were recorded in a lab-built measurement system (Fig. S1, supporting information). An optical fiber (Φ = 1000 μm in diameter) was inserted into the glass tube and to rub the ML powders in an agate mortar. Fiber spectrometers in range of 300–1100 nm (QE pro, Ocean Optics) and 900–1700 nm (NIR Quest 512, Ocean Optics) were used to monitor the ML spectra. The relationship between ML intensity and stress was performed using a universal testing machine (AGS-X, Shimadzu) and a photon detection unit (C9692, Hamamatsu Photonics). Photographs of the samples were taken with a digital camera (EOS 5D Mark II, Canon) and NIR camera (InGaAs C12471-03). Unless otherwise stated, all measurements were performed at room temperature (RT).

Declaration of competing interest

The authors declare that they have no known competing financial interests or personal relationships that could have appeared to influence the work reported in this paper.

Acknowledgements

This work was financially supported by the National Key Research and Development Program (Nos. 2017YFB0404300, 2017YFB0404301), the National Natural Science Foundation of China (Nos. 51872247, 51832005), the Natural Science Foundation of Fujian Province (No. 2018J01080), and the Young Elite Scientists Sponsorship Program by CAST (No. 2018QNRC001).

Appendix A. Supplementary data

Supplementary data to this article can be found online at https://doi.org/10.1016/j.nanoen.2019.104329.

References

[1] X. Wang, H. Zhang, R. Yu, L. Dong, D. Peng, A. Zhang, Y. Zhang, H. Liu, C. Pan, Z. L. Wang, Adv. Mater. 27 (2015) 2324–2331, https://doi.org/10.1002/adma.201405826.
[2] M.J. Soon, S. Seongkyu, S. Hye-Jin, M.C. Won, H. Sung-Ho, G.L. Se, K.L. Sang, Adv. Sustain. Syst. 1 (2017) 1700126, https://doi.org/10.1002/adsu.201700126.
[3] J.C. Zhang, C. Pan, Y.F. Zhu, L.Z. Zhao, H.W. He, X.F. Liu, J.R. Qiu, Adv. Mater. 30 (2018) 9, https://doi.org/10.1002/adma.201804644.
[4] Y. Zuo, X.J. Xu, X. Tao, X. Shi, X.F. Zhou, Z. Gao, X.M. Sun, H.S. Peng, J. Mater. Chem. C 7 (2019) 4020–4025, https://doi.org/10.1039/C9TC00641A.
[5] C.N. Xu, T. Watanabe, M. Akiyama, X.G. Zheng, Appl. Phys. Lett. 74 (1999) 2414–2416, https://doi.org/10.1063/1.123865.
[6] Y.Y. Du, Y. Jiang, T.Y. Sun, J.X. Zhao, B.L. Huang, D.F. Peng, F. Wang, Adv. Mater. 31 (2019) 8, https://doi.org/10.1002/adma.201807062.
[7] D.F. Peng, B. Chen, F. Wang, Chempluschem 80 (2015) 1209–1215, https://doi.org/10.1002/cplu.201500185.
[8] A. Feng, P.F. Smet, Materials 11 (2018) 56, https://doi.org/10.3390/ma11040484.
[9] P. Jha, B.P. Chandra, Luminescence 29 (2014) 977–993, https://doi.org/10.1002/bio.2647.
[10] X.Y. Wei, X. Wang, S.Y. Kuang, L. Su, H.Y. Li, Y. Wang, C. Pan, Z.L. Wang, G. Zhu, Adv. Mater. 28 (2016) 6656–6664, https://doi.org/10.1002/adma.201600604.
[11] L. Li, L. Wondraczek, L. Li, Y. Zhang, Y. Zhu, M. Peng, C. Mao, ACS Appl. Mater. Interfaces 17 (2018) 14509–14516, https://doi.org/10.1021/acsami.8b02530.
[12] H. Kageyama, K. Hayashi, K. Maeda, J.P. Attfield, Z. Hiroi, J.M. Rondinelli, K. R. Poeppelmeier, Nat. Commun. 9 (2018) 15, https://doi.org/10.1038/s41467-018-02838-4.
[13] A. Ishikawa, T. Takata, J.N. Kondo, M. Hara, H. Kobayashi, K. Domen, J. Am. Chem. Soc. 124 (2002) 13547–13553, https://doi.org/10.1021/ja0269643.
[14] M. Almamouri, P.P. Edwards, C. Greaves, M. Slaski, Nature 369 (1994) 382–384, https://doi.org/10.1038/369382a0.
[15] S.X. Li, L. Wang, D.M. Tang, Y.J. Cho, X.J. Liu, X.T. Zhou, L. Lu, L. Zhang, T. Takeda, N. Hirosaki, R.J. Xie, Chem. Mater. 30 (2018) 494–505, https://doi.org/10.1021/acs.chemmater.7b04605.
[16] N. Hirosaki, R.J. Xie, K. Kimoto, T. Sekiguchi, Y. Yamamoto, T. Suehiro, M. Mitomo, Appl. Phys. Lett. 86 (2005) 3, https://doi.org/10.1063/1.1935027.
[17] W.B. Im, S. Brinkley, J. Hu, A. Mikhailovsky, S.P. DenBaars, R. Seshadri, Chem. Mater. 22 (2010) 2842–2849, https://doi.org/10.1021/cm100010z.
[18] K. Ishizaka, M.S. Bahramy, H. Murakawa, M. Sakano, T. Shimojima, T. Sonobe, K. Koizumi, S. Shin, H. Miyahara, A. Kimura, K. Miyamoto, T. Okuda, H. Namatame, M. Taniguchi, R. Arita, N. Nagaosa, K. Kobayashi, Y. Murakami, R. Kumai, Y. Kaneko, Y. Onose, Y. Tokura, Nat. Mater. 10 (2011) 521–526, https://doi.org/10.1038/nmat3051.
[19] P.S. Halasyamani, K.R. Poeppelmeier, Chem. Mater. 10 (1998) 2753–2769, https://doi.org/10.1021/cm980140w.
[20] B.W. Liu, X.M. Jiang, G.E. Wang, H.Y. Zeng, M.J. Zhang, S.F. Li, W.H. Guo, G. C. Guo, Chem. Mater. 27 (2015) 8189–8192, https://doi.org/10.1021/acs.chemmater.5b03649.
[21] Y. Tsujimoto, C.A. Juillerat, W.G. Zhang, K. Fujii, M. Yashima, P.S. Halasyamani, H.C. zur Loye, Chem. Mater. 30 (2018) 6486–6493, https://doi.org/10.1021/acs.chemmater.8b02967.
[22] X.D. Wang, D.F. Peng, B.L. Huang, C.F. Pan, Z.L. Wang, Nano Energy 55 (2019) 389–400, https://doi.org/10.1016/j.nanoen.2018.11.014.
[23] J.H. Hao, C.N. Xu, MRS Bull. 43 (2018) 965–969, https://doi.org/10.1557/mrs.2018.296.
[24] Z.L. Wang, Adv. Funct. Mater. 18 (2008) 3553–3567, https://doi.org/10.1002/adfm.200800541.
[25] Z.L. Wang, Nano Today 5 (2010) 540–552, https://doi.org/10.1016/j.nantod.2010.10.008.
[26] W. Liu, K.T. Lai, K. Eckhardt, Y. Prots, U. Burkhardt, M. Valldor, J. Solid State Chem. 246 (2017) 225–229, https://doi.org/10.1016/j.jssc.2016.11.035.
[27] O. Oeckler, F. Stadler, T. Rosenthal, W. Schnick, Solid State Sci. 9 (2007) 205–212, https://doi.org/10.1016/j.solidstatesciences.2006.11.009.
[28] J.C. Zhang, L.Z. Zhao, Y.Z. Long, H.D. Zhang, B. Sun, W.P. Han, X. Yan, X.S. Wang, Chem. Mater. 27 (2015) 7481–7489, https://doi.org/10.1021/acs.chemmater.5b03570.
[29] J.C. Zhang, C.N. Xu, S. Kamimura, Y. Terasawa, H. Yamada, X.S. Wang, Opt. Express 21 (2013) 12976–12986, https://doi.org/10.1364/OE.21.012976.
[30] J. Botterman, K. Van den Eeckhout, I. De Baere, D. Poelman, P.F. Smet, Acta Mater. 60 (2012) 5494–5500, https://doi.org/10.1016/j.actamat.2012.06.055.
[31] B.L. Huang, M.Z. Sun, D.F. Peng, Nano Energy 47 (2018) 150–171, https://doi.org/10.1016/j.nanoen.2018.02.041.
[32] K. Momeni, G.M. Odegard, R.S. Yassar, J. Appl. Phys. 108 (2010) 7, https://doi.org/10.1063/1.3517095.
[33] Y.F. Hu, Y. Zhang, C. Xu, G.A. Zhu, Z.L. Wang, Nano Lett. 10 (2010) 5025–5031, https://doi.org/10.1021/nl103203u.
[34] S. Gong, W. Schwalb, Y.W. Wang, Y. Chen, Y. Tang, J. Si, B. Shirinzadeh, W. L. Cheng, Nat. Commun. 5 (2014) 8, https://doi.org/10.1038/ncomms4132.
[35] D.J. Lipomi, M. Vosgueritchian, B.C.K. Tee, S.L. Hellstrom, J.A. Lee, C.H. Fox, Z. N. Bao, Nat. Nanotechnol. 6 (2011) 788–792, https://doi.org/10.1038/nnano.2011.184.
[36] C.F. Pan, L. Dong, G. Zhu, S.M. Niu, R.M. Yu, Q. Yang, Y. Liu, Z.L. Wang, Nat. Photonics 7 (2013) 752–758, https://doi.org/10.1038/nphoton.2013.191.

Changjian Chen is currently a postgraduate candidate in College of Materials, Xiamen University. His current research interest focuses on mechanoluminescence materials and their applications in advanced stress sensing.

Dr. Xiandi Wang received his PhD degree in condensed matter physics from the University of Chinese Academy of Sciences in 2016. Now he is an associate professor at Beijing Institute of Nanoenergy and Nanosystems, CAS since 2018. His research interests mainly focus on the fields of piezo-photonic effect and triboelectric nanogenerator for fabricating novel flexible large-scale tactile sensor matrix and stretchable electronics.

Dr. Yixi Zhuang received his PhD from Graduate School of Human and Environmental Studies, Kyoto University in 2014. Now he is an associate professor in College of Materials, Xiamen University. His current research focuses on persistent luminescent materials, mechanoluminescent materials, metal-organic frameworks and their applications for bio-imaging, optical data storage, and advanced anti-counterfeiting.

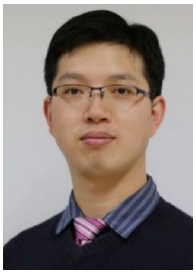

Prof. Caofeng Pan received his B.S. degree (2005) and his Ph. D. (2010) in Materials Science and Engineering from Tsinghua University, China. He then joined the Georgia Institute of Technology as a postdoctoral fellow. He is currently a professor and a group leader at Beijing Institute of Nanoenergy and Nanosystems, Chinese Academy of Sciences since 2013. His main research interests focus on the fields of piezotronics/piezo-phototronics for fabricating new electronic and optoelectronic devices, and self-powered nanosystems. Details can be found at http://www.piezotronics.cn.

Dr. Dong Tu received his PhD degree in materials science and engineering from Kyushu University in 2015. He was employed at National Institute of Advanced Industrial Science and Technology (AIST), Japan, from 2015 to 2017 as a postdoctoral researcher and JSPS researcher. At present, he is a senior researcher of School of Physical Science and Technology, Wuhan University. His research mainly focused on the development of new mechanoluminescence materials, mechanoluminescence mechanism, and the social applications of mechanoluminescence technology.

Prof. Dr. Rong-Jun Xie received his PhD in Shanghai Institute of Ceramics, Chinese Academy of Sciences. Now he is currently a Full Professor in College of Materials, Xiamen University. His research interests include rare-earth-doped nitride phosphors for w-LEDs, luminescent materials for laser-driven white lighting and displays, quantum dots, etc.